

# DIELECTRIC LOADED THz WAVEGUIDE EXPERIMENTALLY OPTIMIZED BY DISPERSION MEASUREMENTS

M. Kellermeier\*, R. W. Assmann<sup>1</sup>, K. Floettmann, F. Lemery  
Deutsches Elektronen-Synchrotron DESY, Germany  
W. Hillert, Universität Hamburg, Hamburg, Germany  
<sup>1</sup>also at Istituto Nazionale di Fisica Nucleare, Frascati, Italy

## Abstract

Emerging high power THz sources pave the road for THz-driven acceleration of ultra-short bunches, and enable their manipulation for diagnostic purposes. Due to the small feature sizes of THz-guiding devices new methods are necessary for their electromagnetic characterization. A new technique has recently been developed which characterizes THz waveguides with respect to their dispersion relations and attenuation. Here, the method is applied to circular waveguides, partially filled with polymer capillaries of different thicknesses, to find a suitable size for THz driven streaking at 287 GHz. Further, rough 3d-printed metallic waveguides are measured to study the effect of roughness on attenuation and phase constant. In general, additive manufacturing techniques show promise for advanced integrated designs of THz driven structures.

## INTRODUCTION

In recent years, there has been growing interest in Terahertz (THz) radiation as driving source for particle accelerators [1–5] due to the availability of emerging laser-based high-power sources [6, 7] and promises in supporting higher field gradients than conventional RF-driven structures. Beyond acceleration, THz driven structures are also studied for beam manipulation, for instance, as transverse deflecting structures [8–12] to measure the bunch length with high resolution. One potential design is based on dielectric loaded waveguides which profit from higher streaking voltage and reduced non-linearities of the field distribution [13, 14]. Due to the small feature size on mm-scale, established characterization methods from radio-frequency structures are difficult to apply. Laser-based techniques partially take over, for instance, in measuring waveguide dispersion [15]. Alternatively, a new RF-based approach has been proposed by the authors to characterize THz structures by their dispersion [16]. The method does not rely on the integrated phase shift, but is able to provide local information within the waveguide.

In the present work, the inner radius of a dielectric loaded waveguide, formed by inserting a polymer capillary in a circular metallic waveguide, is adjusted to match synchronous phase velocity,  $v_{ph} = c$ , to the design frequency of 287 GHz. The design frequency is based on a THz generation setup located at the REGAE facility [13, 17] at DESY. Frequency

tunability of the THz source restricts the waveguide's phase synchronous mode to 286 GHz to 288 GHz.

Further, the dispersion of pure metallic waveguides fabricated by selective laser melting (SLM) is measured. Due to the rough surface the diameter of the cross-section can only be estimated by microscopy. The measured dispersion allows to determine an effective diameter due to the electromagnetic response.

The first chapter briefly recapitulates the experimental setup and the analysis method. In the second chapter, measurements on a metallic waveguide equipped with polymer capillaries are presented. Aiming for a specific design frequency at which the mode propagates synchronously with a potential bunch, the optimal capillary loading is determined. Afterwards, experiments on 3D printed, pure metallic waveguides are shown. Finally, an outlook is given towards an accelerator-based experiment.

## EXPERIMENTAL SETUP AND NETWORK MODEL

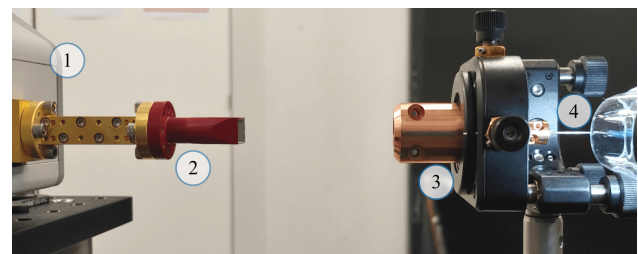


Figure 1: Experimental setup. (1) Extender waveguide port (2) Horn antenna (3) Integrated horn-waveguide structure (4) Movable obstacle. Reproduced from Ref. [16]

The main part of the experimental setup is shown in Fig. 1. Scattering parameters are measured via a Rohde & Schwarz ZVA67 vector network analyzer (not shown) to which a frequency extender ZC330 is connected, spanning the band from 220 GHz to 330 GHz. A pyramidal horn antenna is attached to the waveguide port of the extender. The waveguide under test, which is monolithically integrated with its conical horn coupler, is mounted in a distance of about 7 cm. A reflecting obstacle is placed inside the waveguide from the other side. The obstacle is mounted on a linear translation stage to scan the reflection position in sub-wavelength steps. The position sweep shifts the phase of  $S_{11}$  of the device under test. Multiple reflections between the reference port and the test device distort the S-parameter  $S_{11}^{(m)}$  measured

\* max.kellermeier@desy.de

by the VNA. An error network model has been derived to describe the response. The out-coupling horn, the free space section, and the in-coupling horn are combined into a single error network. The measured response of the total system is modelled as

$$S_{11}^{(m)}(f, l) = a + \frac{b}{e^{-2(\alpha+i\beta)l} - c}, \quad (1)$$

where  $\gamma = \alpha + i\beta$  is the propagation constant, and  $a, b, c$  are parameters combining the error terms, like directivity, source match and reflection tracking. All parameters are frequency dependent. To determine the dispersion relation of the integrated waveguide, the measured set  $S_{11}^{(m)}(l; f)$  is analyzed independently for each frequency point. The model Eq. (1) is fitted via a non-linear least-squares method to each  $S_{11}^{(m)}(l)$ , where eight real unknown parameters are taken into account. The error terms are complex-valued. If the scanning range is not sufficient to resolve the attenuation, the parameter space can be reduced to seven unknowns since  $\alpha = 0$  is assumed.

### WAVEGUIDES LOADED WITH 3D PRINTED POLYMER CAPILLARIES

The split-block waveguide presented in [16] is successfully loaded with six additively manufactured polymer capillaries. The waveguide has an experimentally determined radius of  $(0.66 \pm 0.01)$  mm. The capillaries are printed by the ASIGA MAX X UV385 DLP printer. Moiin Tech Clear has been chosen as resin and its permittivity has been measured in advance,  $\epsilon_r = 2.92 \pm 0.02$ . Using the design frequency, outer radius and permittivity, the required inner radius  $a$  to achieve  $v_{ph} = c$  is calculated analytically. Due to the uncertainty in  $\epsilon_r$  and potential air gaps between capillary and metallic wall, the measured phase synchronous frequency may deviate substantially. Therefore, the capillaries have been printed with varying radii close to the design value,

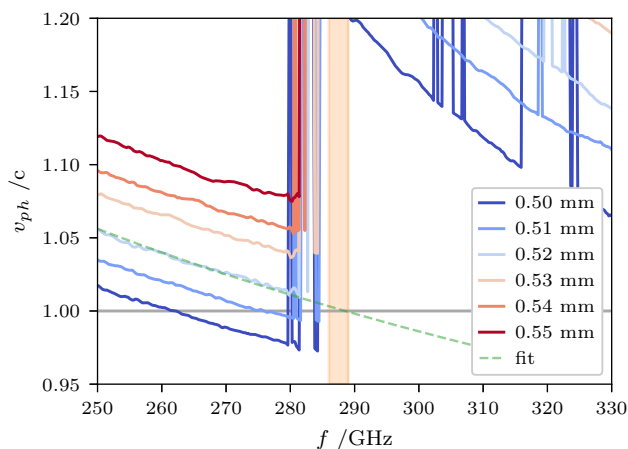


Figure 2: Phase velocity dispersion of the dielectric loaded waveguide with polymer capillaries of different size as lining. The fit of the third measurement approximates  $v_{ph}(f)$  with Eq. (2). The orange region marks the goal frequency band.

covering the range from 0.5 mm to 0.55 mm. The actual size may deviate due to shrinkage. But the goal is to optimize the parameters adjustable for the printing process.

Figure 2 shows the measured phase velocity dispersion for the six waveguides of different polymer size, focusing on the frequency range and phase velocity range of interest. First, it is observed that in all waveguides higher order modes are predominantly excited above  $\approx 280$  GHz. The current model in Eq. (1) assumes a single-mode excitation which is why it is the modes are not separated. Further, the first two measurements,  $a = 0.5$  mm and  $a = 0.51$  mm, show a crossing of the speed of light dispersion already below the higher order mode threshold. The fundamental  $HE_{11}$  mode propagates phase synchronously with a hypothetical ultra-relativistic beam at  $(262 \pm 2)$  GHz and  $(276 \pm 2)$  GHz. Both cases demonstrate the feasibility of the method, but the frequencies lie outside the tunability range of the dedicated THz source. Although the third dispersion line shows the jump to a higher order mode, its course indicates a crossing of  $v_{ph} = c$  by extrapolation from the data points below the jump. A non-linear least-squares fit is applied to the truncated data, using the approximate model

$$v_{ph}(f) = p_0 + \frac{p_1}{f}, \quad (2)$$

where  $p_0, p_1$  are the fit parameters. This approximation is valid in the vicinity of  $v_{ph} = c$  and the thickness of the dielectric  $b - a$  must be smaller than the inner radius. The fit is plotted in Fig. 2 and a crossing of  $v_{ph} = c$  is found in the frequency range of interest, close to 287 GHz. Although the higher order mode is mainly excited, it is reasonable to assume that the fundamental mode is also excited substantially. The capillary with  $a = 0.52$  mm mounted in the metallic waveguide is suitable for future experiments involving THz-beam interaction.

### METALLIC 3D PRINTED WAVEGUIDES

The experimental method is also applied to characterize horn-waveguide devices fabricated by additive manufacturing of steel (316L), also called metallic 3D-printing. The waveguides have been designed with varying inner radius between 0.75 mm to 0.95 mm to achieve phase velocities close

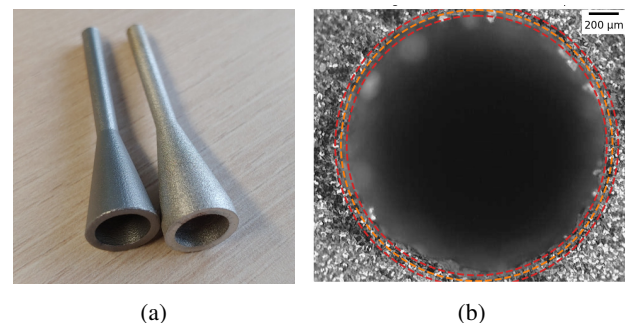


Figure 3: (a) Photograph of two 3D-printed steel waveguides. (b) Microscope image of the largest waveguide.

to  $c$ . Figure 3(a) shows a photograph of two of the five studied devices. Each waveguide has been inspected by microscopy in advance of the dispersion measurement. The microscope image of the largest waveguide is shown in Fig. 3(b) as an example. A rough surface is observed, making it difficult to make out a clear edge. The overlaid circles estimate the aperture size to be  $(0.91 \pm 0.04)$  mm in radius. While the range of uncertainty covers the designed radius of 0.95 mm it will be shown later that the deviation is systematic. The uncertainty reflects the surface variation.

Figure 4 shows the analysis of the five measurements. The increase in cross-section size goes along with a decreasing phase velocity, as expected. Due to the comparably large dimensions the waveguides are all inherently overmoded which is not only observable as jumps to higher order modes. For instance,  $v_{ph}(f)$  of the 0.95 mm waveguide shows wiggles below 280 GHz which are explained by multimode excitation. The fit of Eq. (1) is less accurate if the analyzed signal  $S_{11}(l)$  shows a strong beat pattern. The same wiggles are observed even for the small aperture waveguide,  $a = 0.75$  mm, but only above 280 GHz.

The dispersion relations can be utilized to determine an effective radius by fitting the analytic dispersion model of a purely metallic waveguide. The data points are truncated at the jump for the least-squares method in order to restrict the data to a single mode. Table 1 lists the nominal design radii, the radii determined by microscopy, and the radii derived as fit parameter. All measured radii, both by microscopy and dispersion relation, are smaller than the design value. In the first case, the analysis is imprecise due to the rough surface. Assuming the effective radius is close to the mechanical radius, the measurements reveal a systematic deviation of about 0.07 mm. This indicates a misconfiguration of the SLM machine, which has later been confirmed by internal quality assurance and by the manufacturer's maintenance.

As purely metallic waveguides the 3D-printed structures are not directly applicable to beam based experiments without further modification since  $v_{ph} > c$ . Further, surface roughness must be reduced since a significant amount of power is dissipated otherwise. As an example, the atten-

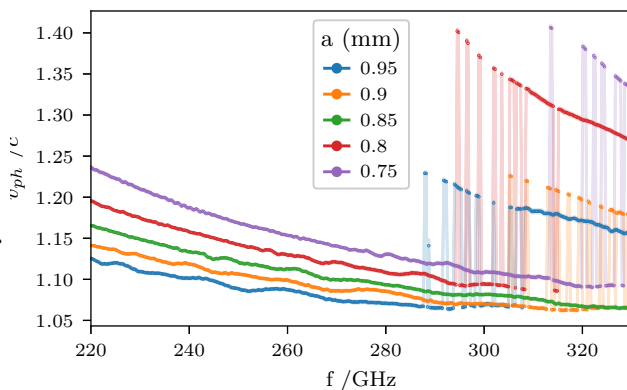


Figure 4: Measured dispersion,  $v_{ph}(f)$ , for five steel waveguides with varying inner radius.

Table 1: Dimensions of the steel waveguides: Nominal radius as foreseen in the CAD model, radius obtained from circle detection in microscopy images (Fig. 3(b)), fit parameter of the dispersion curve. Experimental uncertainty in  $a$  evaluated by Monte Carlo sampling is below 1  $\mu$ m.

No.	nominal (mm)	microscopy (mm)	Fit (mm)
1	0.75	$0.69 \pm 0.06$	0.678
2	0.8	$0.71 \pm 0.06$	0.727
3	0.85	$0.80 \pm 0.04$	0.776
4	0.90	$0.88 \pm 0.05$	0.824
5	0.95	$0.91 \pm 0.04$	0.876

uation of a smaller printed waveguide ( $a = 0.45$  mm) has been analyzed, resulting in  $\alpha \approx 15$  Np  $m^{-1} = 130$  dB  $m^{-1}$  at the central frequency. Assuming a bulk conductivity of  $1.3 \times 10^6$  S  $m^{-1}$ , the attenuation would be about 7 Np  $m^{-1} = 60$  dB  $m^{-1}$  if the surface were perfectly smooth. The roughness is measured by a profilometer,  $R_a = 8$   $\mu$ m,  $R_z = 50$   $\mu$ m.

## CONCLUSION AND OUTLOOK

A dielectric loaded waveguide has been optimized with respect to the phase synchronous frequency by varying the dimensions of the dielectric layer. The polymer capillary with an inner radius of 0.52 mm satisfies the condition of  $v_{ph}(287 \text{ GHz}) = c$  for the fundamental mode. Due to phase slippage, excited higher order modes will have no net effect on a potential electron bunch but lower the energy coupled to the preferred fundamental mode. Due to mechanical constraints the optimized waveguide presented here cannot be utilized as transverse deflecting structure for the planned experiment at the REGAE facility. At the time of writing, a new waveguide is being manufactured which fits inside the experimental chamber, and potentially mitigates the excitation of higher order modes. Following the present work, the dimensions of the dielectric capillary will be optimized for 287 GHz, taking into consideration that the beam at REGAE is not ultra-relativistic.

The current status of metallic 3D-printing requires further surface finishing, like electropolishing, and studies to improve their performance as THz waveguides. The experimental setup supports these efforts, providing insights on the fabricated devices. Here, the dispersion relation led to an effective radius which strongly deviates from the design value.

## ACKNOWLEDGEMENTS

The authors are grateful for technical support from O. Rasmussen and F. Borges, and feedback from MPY-1 colleagues. Special thanks go to F. Burkart for internal review of the manuscript. This work has been supported by the European Research Council under the European Union's Seventh Framework Programme (FP/2007-2013)/ERC Grant No. 609920. All figures and pictures by the authors are published under a CC-BY license.

## REFERENCES

- [1] E. A. Nanni *et al.*, “Terahertz-driven linear electron acceleration,” *Nat. Commun.*, vol. 6, p. 8486, 2015, issn: 2041-1723. doi:10.1038/ncomms9486.26439410
- [2] F. Lemery, K. Floettmann, P. Piot, F. X. Kärtner, and R. Aßmann, “Synchronous acceleration with tapered dielectric-lined waveguides,” *Phys. Rev. Accel. Beams*, vol. 21, no. 5, p. 051302, May 25, 2018. doi:10.1103/PhysRevAccelBeams.21.051302.
- [3] T. Vinatier, R. W. Assmann, U. Dorda, F. Lemery, and B. Marchetti, “Simulation of a concept for a compact ultrafast X-ray pulse source based on RF and THz technologies,” *J. Appl. Phys.*, vol. 125, no. 16, p. 164901, Apr. 28, 2019, issn: 0021-8979, 1089-7550. doi:10.1063/1.5091109
- [4] M. T. Hibberd *et al.*, “Acceleration of relativistic beams using laser-generated terahertz pulses,” *Nat. Photonics*, vol. 14, no. 12, pp. 755–759, Aug. 10, 2020, issn: 1749-4893. doi:10.1038/s41566-020-0674-1
- [5] H. Tang *et al.*, “Stable and Scalable Multistage Terahertz-Driven Particle Accelerator,” *Phys. Rev. Lett.*, vol. 127, no. 7, p. 074801, Aug. 12, 2021. doi:10.1103/PhysRevLett.127.074801.
- [6] F. Lemery *et al.*, “Highly scalable multicycle THz production with a homemade periodically poled macrocrystal,” *Commun. Phys.*, vol. 3, no. 1, pp. 1–8, Aug. 28, 2020, issn: 2399-3650. doi:10.1038/s42005-020-00421-2
- [7] H. Olgun *et al.*, “Highly efficient narrowband terahertz generation driven by a two-spectral-line laser in PPLN,” *Opt. Lett.*, Mar. 3, 2022, issn: 0146-9592, 1539-4794. doi:10.1364/OL.448457
- [8] J. Fabiańska, G. Kassier, and T. Feurer, “Split ring resonator based THz-driven electron streak camera featuring femtosecond resolution,” *Sci. Rep.*, vol. 4, no. 1, p. 5645, Jul. 10, 2014, issn: 2045-2322. doi:10.1038/srep05645
- [9] C. Kealhofer, W. Schneider, D. Ehberger, A. Ryabov, F. Krausz, and P. Baum, “All-optical control and metrology of electron pulses,” *Science*, vol. 352, no. 6284, pp. 429–433, Apr. 22, 2016. doi:10.1126/science.aae0003
- [10] D. Zhang *et al.*, “Segmented terahertz electron accelerator and manipulator (STEAM),” *Nat. Photonics*, vol. 12, no. 6, pp. 336–342, Jun. 2018, issn: 1749-4885, 1749-4893. doi:10.1038/s41566-018-0138-z
- [11] F. Lemery, R. Aßmann, K. Flöttmann, and T. Vinatier, “A Transverse Deflection Structure with Dielectric-Lined Waveguides in the Sub-THz Regime,” in *Proc. IPAC’17*, Copenhagen, Denmark, May 2017, pp. 215–218. doi:10.18429/JACoW-IPAC2017-MOPAB052
- [12] L. Zhao *et al.*, “Terahertz Streaking of Few-Femtosecond Relativistic Electron Beams,” *Phys. Rev. X*, vol. 8, no. 2, p. 021061, Jun. 8, 2018. doi:10.1103/PhysRevX.8.021061
- [13] F. Mayet, “Acceleration and Phase Space Manipulation of Relativistic Electron Beams in Nano- and Micrometer-Scale Dielectric Structures,” Ph.D. dissertation, Verlag Deutsches Elektronen-Synchrotron, 2019. <https://bib-pubdb1.desy.de/record/426707>
- [14] V. Paramonov and K. Floettmann, “Lower limit of the transverse emittance growth in deflecting rf fields,” *Phys. Rev. Accel. Beams*, vol. 23, no. 1, p. 014401, Jan. 9, 2020. doi:10.1103/PhysRevAccelBeams.23.014401
- [15] V. Georgiadis, A. L. Healy, M. T. Hibberd, G. Burt, S. P. Jamison, and D. M. Graham, “Dispersion in dielectric-lined waveguides designed for terahertz-driven deflection of electron beams,” *Appl. Phys. Lett.*, vol. 118, no. 14, p. 144102, Apr. 5, 2021, issn: 0003-6951. doi:10.1063/5.0041391
- [16] M. Kellermeier, F. Lemery, K. Floettmann, W. Hillert, and R. Aßmann, “Self-calibration technique for characterization of integrated THz waveguides,” *Phys. Rev. Accel. Beams*, vol. 24, no. 12, p. 122001, Dec. 6, 2021. doi:10.1103/PhysRevAccelBeams.24.122001
- [17] S. Manz *et al.*, “Mapping atomic motions with ultrabright electrons: Towards fundamental limits in space-time resolution,” *Faraday Discuss.*, vol. 177, no. 0, pp. 467–491, 2015. doi:10.1039/C4FD00204K